

Suppression of luminosity and mass–radius relation of highly magnetized white dwarfs

Abhay Gupta,^{1★} Banibrata Mukhopadhyay^{1★} and Christopher A. Tout^{2★}

¹Department of Physics, Indian Institute of Science, Bangalore 560012, India

²Institute of Astronomy, The Observatories, Medingley Road, Cambridge CB3 0HA, UK

Accepted 2020 June 2. Received 2020 April 22; in original form 2020 February 14

ABSTRACT

We explore the luminosity L of magnetized white dwarfs and its effect on the mass–radius relation. We self-consistently obtain the interface between the electron degenerate-gas dominated inner core and the outer ideal gas surface layer or envelope by incorporating both the components of gas throughout the model white dwarf. This is obtained by solving the set of magnetostatic equilibrium, photon diffusion, and mass conservation equations in the Newtonian framework, for different sets of luminosity and magnetic field. We appropriately use magnetic opacity, instead of Kramer’s opacity, wherever required. We show that the Chandrasekhar limit is retained, even at high luminosity up to about $10^{-2} L_{\odot}$ but without magnetic field, if the temperature is set constant inside the interface. However, there is an increased mass for large-radius white dwarfs, an effect of photon diffusion. Nevertheless, in the presence of strong magnetic fields, with central strength of about 10^{14} G, super-Chandrasekhar white dwarfs, with masses of about $1.9 M_{\odot}$, are obtained even when the temperature inside the interface is kept constant. Most interestingly, small-radius magnetic white dwarfs remain super-Chandrasekhar even if their luminosity decreases to as low as about $10^{-20} L_{\odot}$. However, their large-radius counterparts in the same mass–radius relation merge with Chandrasekhar’s result at low L . Hence, we argue for the possibility of highly magnetized, low luminous super-Chandrasekhar mass white dwarfs that, owing to their faintness, can be practically hidden.

Key words: equation of state – opacity – radiation mechanisms: general – stars: luminosity function, mass function – white dwarfs – magnetic fields.

1 INTRODUCTION

Observations of several overluminous Type Ia supernovae (SNe Ia), see Howell et al. 2006; Scalzo et al. 2010; Silverman et al. 2011, imply the existence of super-Chandrasekhar white dwarfs. It was shown earlier (Das & Mukhopadhyay 2012, 2013; Subramanian & Mukhopadhyay 2015) that white dwarfs with highly super-Chandrasekhar mass, $M > M_{\text{Ch}} = 1.44 M_{\odot}$, are possible when rotation and magnetic fields are taken into consideration. It was also shown (Das & Mukhopadhyay 2012, 2013) that when the magnetic field is greater than a critical strength of 4.414×10^{13} G, such that the Larmor radius is the same order of, or smaller than, the Compton wavelength of the electrons, the effect of Landau quantization becomes important and thus modifies the equation of state (EoS) of the electron-degenerate matter of the white dwarf. This modified EoS further gives rise to super-Chandrasekhar white dwarfs and a new limit of $2.58 M_{\odot}$. Interestingly, Sloan Digital Sky Survey (SDSS) data (Vanlandingham et al. 2005) indicate that

magnetic samples of white dwarfs span the same temperature range as non-magnetic white dwarfs and support the claim that magnetic white dwarfs tend to have larger masses compared to their non-magnetic counterparts.

The existence of magnetic white dwarfs (hereinafter B-WDs) does not just explain super-Chandrasekhar mass progenitors of overluminous SNe Ia, but also B-WDs correspond to soft gamma-ray repeaters (SGRs) and anomalous X-ray pulsars (AXPs) with much lower magnetic fields than magnetars (Mukhopadhyay & Rao 2016). Further, the glitch and antiglitch of the source 1E 2259+586 may be explained based on the stiffness of the magnetic field profile, mass-loss, and rotational energy extraction rates of a B-WD. Moreover, the peculiar radio transient of GCRT J1745–3009 can be interpreted as a white dwarf pulsar (WDP) based on the B-WD model because its larger magnetic field and smaller radius could prove it is of low luminosity and further away, and hence dimmer and able to evade detection.

However, the questions remain: Why have not enough B-WDs yet been seen directly and why have only about a dozen overluminous SNe Ia implying super-Chandrasekhar white dwarfs been seen so far? While Das, Mukhopadhyay & Rao (2013) attempted to address

* E-mail: abhaygupta06@gmail.com (AG); bm@iisc.ac.in (BM); cat@ast.cam.ac.uk (CAT)

these questions by arguing that they are rare objects as overluminous SNe Ia, Bhattacharya, Mukhopadhyay & Mukerjee (2018) explored their luminosity with the model described by Shapiro & Teukolsky (1983) for nonmagnetic white dwarfs. Based on the photon-diffusion equation and the magnetostatic balance condition, and assuming that interface parameters remain unaffected between B-WDs and nonmagnetic white dwarfs, Bhattacharya, Mukhopadhyay & Mukerjee (2018) found that, for a given age, the luminosity of B-WDs decreases significantly, from about 10^{-6} to $10^{-9} L_{\odot}$ when the magnetic field strength increases from about 10^9 to 10^{12} G at the interface and hence the envelope. In fact, Valyavin et al. (2014), based on an optical observation, showed that the strong magnetic field suppresses convection over the entire surface in magnetic white dwarfs, which decreases luminosity and increases cooling time-scale significantly. They analysed about 8-yr observed data and obtained brightness and magnetic field of WD 1953–011, which is a cool white dwarf. Their results argue that the magnetic fields are expected to be common in cool, hence low luminous, white dwarfs and B-WDs are actually too young and low luminous. Indeed, in the theoretical ground, Bhattacharya, Mukhopadhyay & Mukerjee (2018) found the cooling rates corresponding to luminosities from about 10^{-6} to $10^{-9} L_{\odot}$. In this way, they studied the effect of luminosity on the outer surface layer of the white dwarf, where only ideal gas pressure exists. Because the interface between the electron-degenerate core and the surface layer or envelope is very close to the surface of the white dwarf, the mass at the interface was chosen to be the total mass of the corresponding white dwarf. Thus, the characteristics of the white dwarf were obtained by solving the two differential equations of magnetohydrostatic equilibrium and photon diffusion. While this was a very good start, the choice of the same interface parameters for B-WDs and nonmagnetic white dwarfs is a big assumption. Moreover, the results based on modelling only the envelope with preassigned mass and radius should also be taken with caution because B-WD masses and luminosities are yet to be established.

Here we remove all the above assumptions and find the mass–radius relation along with luminosity of B-WDs self-consistently. Earlier, the mass–radius relation was rigorously explored in Newtonian (Das & Mukhopadhyay 2012; Das, Mukhopadhyay & Rao 2013) as well as general relativistic (Das & Mukhopadhyay 2014, 2015; Subramanian & Mukhopadhyay 2015; Mukhopadhyay, Rao & Bhatia 2017) formalisms in various magnetic field and rotational configurations, by our group. Some of these works considered poloidally as well as toroidally dominated magnetic field geometries and obtained similar results showing the existence of super-Chandrasekhar white dwarfs (also see, e.g. Boshkayev et al. 2013; Franzon & Schramm 2015; Carvalho et al. 2018). Recently, Otoniel et al. (2019) revisited the problem again rigorously in general relativistic frameworks with dipole fields but, more importantly, considering possible instability of the matter with respect to pycnonuclear and electron capture reactions. Such stability criteria, particularly of pycnonuclear reactions, were not considered by our group in order to establish the mass–radius relation mentioned above. However, still Otoniel et al. (2019) found the maximum mass of non-rotating B-WDs to be $2.14 M_{\odot}$ with central magnetic field $\sim 3.85 \times 10^{14}$ G with limiting central density $9.35 \times 10^9 \text{ g cm}^{-3}$, when rotation certainly would increase the mass further. According to them, above this density, pycnonuclear fusion reactions destabilize the star. This work further establishes strongly the idea of the existence of significantly super-Chandrasekhar white dwarf with a new mass limit, which we initiated in 2012 with a simpler model and evolved over the years with the introduction of rigorous physics. Nevertheless, all the work neglected any

possible variation of temperature in the star and its effect in the mass–radius relations. However, this is very important when luminosity of B-WDs is also planned to be explored and the aim is to understand why super-Chandrasekhar white dwarfs are hardly visible. Bhattacharya, Mukhopadhyay & Mukerjee (2018) included temperature gradient in assessing luminosity of B-WDs, but they did not explore mass–radius relation and confined their physics in the envelope strictly. Theirs was just one step forward compared to white dwarf luminosity investigated by Shapiro & Teukolsky (1983) without magnetic fields. In this work, we have removed such limitations.

We model the star throughout, from the core to surface, with the finite temperature gradient in envelope determining the underlying luminosity with total pressure as the sum of the electron degenerate, ideal gas, and magnetic pressures. Naturally, the correct modelling leads to the dominance of electron-degenerate pressure over ideal gas pressure in core and otherwise in the envelope. The radius where the ideal gas pressure dominates the degenerate pressure is defined to be the interface. We begin to solve the three differential equations for magnetostatic equilibrium, mass conservation, and photon diffusion. As we mainly venture (strongly) magnetized white dwarfs, we neglect any possible convection as strong field suppresses convection effects (e.g. Canuto & Mazzitelli 1992; Solanki 2003). Moreover, we use magnetic opacity instead of Kramer’s opacity, wherever necessary.

In the next section we give an overview of the procedure to self-consistently obtain the interface of the B-WD. In Section 3, we describe the mass–radius relation including the effects of luminosity and, hence, finite temperature gradient, and magnetic fields. Subsequently, in Section 4, we attempt to reinterpret the results based on total energy conservation. In Section 5, we summarize the results and we conclude the work in Section 6.

2 WHITE DWARF AND ITS INTERFACE

We describe the conditions used and equations solved to formulate a method to self-consistently obtain the structure of B-WDs and the interface between the inner electron-degenerate core and outer ideal gas envelope. For the present purpose, we neglect any general relativistic effect as it is not expected to influence luminosity, which mostly is the envelope phenomena. Moreover, as the main plan is to target significantly super-Chandrasekhar white dwarfs, a possible slight change in mass using general relativistic framework compared to their Newtonian counterpart does not matter. Therefore, the model equations describing magnetostatic equilibrium, photon diffusion, and mass conservation, approximating stars to be spherical without losing any physics for the present purpose, respectively, are

$$\frac{d}{dr}(P_{\text{degenerate}} + P_B + P_{\text{ideal}}) = -\frac{Gm(r)}{r^2}(\rho + \rho_B), \quad (1)$$

$$\frac{dT}{dr} = -\frac{3}{4ac} \frac{\kappa(\rho + \rho_B)}{T^3} \frac{L_r}{4\pi r^2}, \quad (2)$$

$$\frac{dm}{dr} = 4\pi r^2(\rho + \rho_B). \quad (3)$$

In these equations, $P_{\text{degenerate}}$ and P_{ideal} are the electron degeneracy pressure established by Chandrasekhar (1935) and the ideal gas pressure ($\rho kT/\mu m_p$), where ρ is the density of the matter, k Boltzmann’s constant, T the temperature, $\mu \approx 2$ the mean molecular weight and m_p the mass of proton, respectively, m the mass enclosed at radius r , G the Newton’s gravitation constant, a the radiation constant, c the speed of light, L_r the luminosity at radius r , κ the opacity, P_B and ρ_B the contributions from magnetic field to the pressure and density, respectively, and r the distance from

the centre of star. As we restrict central magnetic field to $\sim 10^{14}$ G, the assumption of spherical star is approximately justified (Subramanian & Mukhopadhyay 2015).

It is well known that compact stars with strong magnetic fields (e.g. magnetars, B-WDs) tend to have additional pressure and density contributions owing to the magnetic field, which can be denoted by $P_B = B^2/8\pi$, where field $B = \sqrt{\mathbf{B}\cdot\mathbf{B}}$, with \mathbf{B} being magnetic field vector, and $\rho_B = B^2/8\pi c^2$ (Sinha, Mukhopadhyay & Sedrakian 2013; Das & Mukhopadhyay 2014; Bhattacharya et al. 2018). The opacity for a non-magnetized white dwarf is approximated by Kramers' formula, $\kappa = \kappa_0 \rho T^{-3.5}$, where $\kappa_0 = 4.34 \times 10^{24} Z(1+X) \text{ cm}^2 \text{ g}^{-1}$ and X and Z are the mass fractions of hydrogen and heavy elements (elements other than hydrogen and helium) in the stellar interior. For a typical white dwarf, $X = 0$, and we assume, for simplicity, the mass fraction of helium $Y = 0.9$ and $Z = 0.1$. The opacity is due to the bound-free and free-free transitions of electrons (Shapiro & Teukolsky 1983). In the presence of B , the variation of radiative opacity with B can be modelled similarly to neutron stars as $\kappa = \kappa_B \approx 5.5 \times 10^{31} \rho T^{-1.5} B^{-2} \text{ cm}^2 \text{ g}^{-1}$ (Ventura & Potekhin 2001), with the condition that radiative opacity should be dominant and $B/10^{12} \text{ G} \geq T/10^6 \text{ K}$, otherwise Kramers' formula should be used. For the profile of magnetic field inside the B-WD, we use the profile used earlier extensively for magnetized neutron stars and B-WDs (Bandyopadhyay, Chakrabarty & Pal 1997; Das & Mukhopadhyay 2014) given by

$$B \left(\frac{\rho}{\rho_0} \right) = B_s + B_0 \left[1 - \exp \left(-\eta \left(\frac{\rho}{\rho_0} \right)^\gamma \right) \right], \quad (4)$$

where ρ_0 is a measure of density (chosen roughly 10 per cent of the central matter density of the corresponding white dwarf), B_s is the surface magnetic field, B_0 is a parameter with dimension of magnetic field, and η and γ are dimensionless parameters that determine how exactly the field decays from the centre to surface. This can be parametrized (Das & Mukhopadhyay 2014) with suitable constraints on pressure. Note that, as $\rho \rightarrow 0$ close to the surface of the white dwarf, $B \rightarrow B_s$. For our work, the parameters are selected to be $\rho_0 = 10^9 \text{ g cm}^{-3}$, $\eta = 0.8$, and $\gamma = 0.9$ following Bhattacharya, Mukhopadhyay & Mukerjee (2018). Also, B_s and B_0 are chosen based on previous work and observations (Das & Mukhopadhyay 2014; Bhattacharya, Mukhopadhyay & Mukerjee 2018).

In order to obtain a solution, luminosity is taken to be constant for simplicity and because there is no hydrogen burning or nuclear fusion taking place to power the white dwarf, so that $L_r = L$. Note that, in principle, convection may transfer a significant fraction of the total energy flux depending on magnetic field strength. It is however also known (e.g. Canuto & Mazzitelli 1992; Solanki 2003) that a strong field significantly inhibits convection. As the present venture is mostly to analyse strong field effects in white dwarfs, when even the weakest chosen surface field is no less than 10^7 G , we can safely ignore convection from the model equations. Koester & Chanmugam (1990) argued that, if the luminosity is considered to be constant, it is preferred to integrate the differential equations from the surface towards the centre. The surface is defined by the corresponding radius of the white dwarf. In order to solve for the set of differential equations, here by a Runge-Kutta method, the different parameters such as temperature, mass, and density at the surface must be supplied. The surface temperature is obtained from the Stefan-Boltzmann law, $T_s = (L/4\pi R^2 \sigma)^{1/4}$, for different luminosities L and the corresponding radii R , when σ is the Stefan-Boltzmann constant. The surface density, which has to be several orders of magnitude smaller than the central density, is chosen such

that the equations can be solved simultaneously within the tolerance limits, because both 1 and $10^{-10} \text{ g cm}^{-3}$ can be considered to be quite small compared to $10^4\text{--}10^9 \text{ g cm}^{-3}$ (the range of central densities for white dwarfs). The optimum range comes out to be 10^{-6} to $10^{-9} \text{ g cm}^{-3}$ and we choose $10^{-7} \text{ g cm}^{-3}$ as the surface density for all the cases. We have checked that the results are unaffected by any minor change in the surface density within the above range. Further, the mass is obtained with a shooting method by iteratively solving the equation set to satisfy the condition that the mass obtained close to the centre, at 10 km from the centre, integrating from surface is the same as that obtained by solving the mass conservation equation (3), given the solution for density profile. In this way, we obtain the mass for a given radius of a white dwarf.

Now we can self-consistently obtain the interface, which is defined to be the radius at which the ideal gas pressure starts to dominate over the degenerate pressure. An example has been discussed in the Appendix to further clarify how the interface of a white dwarf is obtained in our method. It is known that the interior of a white dwarf consists completely of degenerate gas. The electrons have a large mean-free path because of the filled Fermi sea, so there is a high thermal conductivity and hence a uniform temperature (Shapiro & Teukolsky 1983). Thus, another condition can be imposed that the right-hand side of photon-diffusion equation (2) is zero from the interface to centre and we study its effects on the mass-radius solution. We obtain interesting results on implementing this condition in non-magnetized white dwarfs. Hence, there are two possible solution cases: (1) The photon-diffusion equation (2) is valid throughout the white dwarf, and (2) $dT/dr = 0$ for radii less than the interface radius. However, both cases produce a very similar interface radius.

2.1 Non-magnetic results

First, we investigate the effect of a finite temperature gradient in the stellar structure without magnetic fields. Fig. 1 shows how the photon-diffusion equation, the temperature gradient, modifies the mass-radius relation compared to Chandrasekhar's original results (Chandrasekhar 1935), when $dT/dr \neq 0$ throughout, the first condition above. We find that there is a shift in the mass-radius relation towards increasing mass and radius compared to the case with $dT/dr = 0$ throughout. It shows super-Chandrasekhar masses for smaller radii. However, there seems to be enough evidence that, in the absence of magnetic fields and rotation, the Chandrasekhar limit is preserved. By imposing the second condition above, we see that indeed the Chandrasekhar limit is retained but there is an overall increase in mass in the larger radius regime in the mass-radius relation compared to Chandrasekhar's. This is similar to the earlier finding of increasing mass seen at larger radii, while preserving Chandrasekhar's limit, at higher temperatures with the finite temperature electron-degenerate EoS (see fig 4. of Boshkayev et al. 2016) and the same is confirmed by SDSS. Therefore, the first condition above seems physically implausible. Note that in either of the cases, increasing luminosity leads to more deviation of the mass-radius relation with increasing mass (and radius for the first case). This is expected because higher luminosity indicates higher thermal energy leading to higher ideal gas pressure, allowing the white dwarf to hold more mass.

Table 1 lists the central and interface temperatures and densities for some white dwarf solutions of various masses and radii. It can be inferred that, for a particular radius of the white dwarf, increasing the luminosity increases the effective thermal energy or

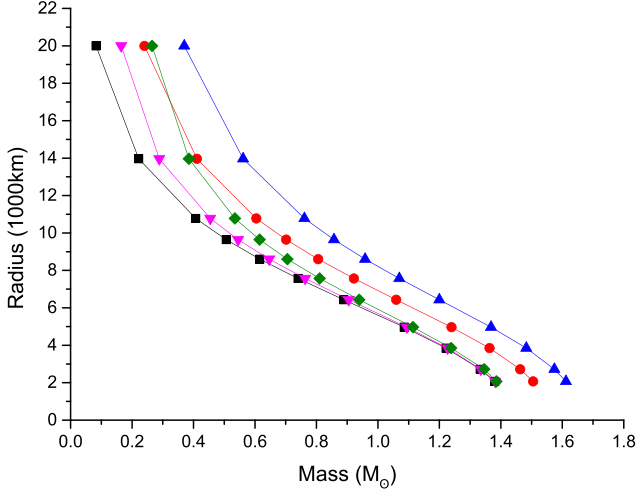


Figure 1. The effect of radiative energy transport on the mass–radius relation, for constant temperature throughout, Chandrasekhar’s results (black squares), non-zero dT/dr throughout for $10^{-2} L_{\odot}$ (blue upward triangles) and $10^{-4} L_{\odot}$ (red circles), and $dT/dr = 0$ below the interface radius for $10^{-2} L_{\odot}$ (green diamonds) and $10^{-4} L_{\odot}$ (magenta downward triangles).

temperature, leading to a larger size of the surface layer or envelope. This, in turn, decreases the interface radius in order to hold the excess thermal energy. Note that including the radiative transport of energy increases the central density and so also the mass, compared to Chandrasekhar’s results (Chandrasekhar 1935). However, for smaller radii, when we make the temperature constant below the interface radius, condition (2) above, the increase in central density is not significant so that the Chandrasekhar limit is preserved. This is also because the surface layer is smaller for smaller white dwarfs because they are more dominated by electron-degenerate matter.

3 EFFECT OF MAGNETIC FIELD

In order to understand how magnetic field affects the white dwarf structure, we first investigate its effect on the magnetostatic equilibrium equation (1) and mass conservation equation (3) with $P_{\text{ideal}} = 0$, without the photon-diffusion equation (2). It is seen from Fig. 2 that B_0 plays the crucial role and it has to be large enough for any significant change in the mass–radius relation. Hence, except for the cases with $(B_s, B_0) = (10^9, 10^{14})$ G (red circles) and $(10^7, 10^{14})$ G (yellow stars), all the results practically overlap.

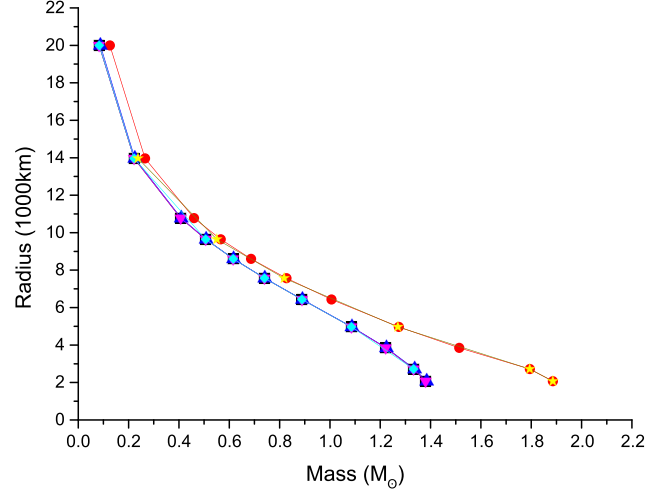


Figure 2. The effect of magnetic field to the mass–radius relation, for zero field, Chandrasekhar’s results (black squares), $(B_s, B_0) = (10^9, 10^{14})$ G (red circles), $(10^9, 10^{13})$ G (blue upwards triangles), $(10^9, 10^{12})$ G (sky diamonds), $(10^7, 10^{14})$ G (yellow stars), and $(10^7, 10^{12})$ G (magenta downward triangles).

Now if we include the photon-diffusion equation (2) in the computation, Figs 3 and 4 show how the magnetic field, along with luminosity, affects the mass–radius relation for conditions (1) and (2) above. Only strong central magnetic fields significantly affect the mass of a white dwarf for a given radius. The mass–radius relations with central field $\sim 10^{14}$ G merge at high mass (central density) regime exceeding Chandrasekhar’s limit, as shown by the lines with blue upward triangles and yellow stars in Figs 3 and 4. Moreover, all other mass–radius relations of lower central fields also overlap with each other independent of magnetic fields, particularly in the high-mass (central density) regime, restricted by Chandrasekhar’s limit. However, the mass–radius curve with $dT/dr = 0$ throughout (without contribution of photon diffusion) and without magnetic field, i.e. Chandrasekhar’s result, shown by the line with black squares is uniquely separated from other curves, as shown in Fig. 3. This confirms that temperature gradient and magnetic fields both have distinct effects in white dwarfs. However, Fig. 4 shows that photon diffusion with isothermal core ($dT/dr = 0$ below the interface), with lower central magnetic fields $< 10^{14}$ G, only affects the mass–radius relation at the low-mass (density) regime slightly, leading to increasing radius for a given mass (see lines with red circles, magenta downward triangles, sky diamonds, and green cross). In

Table 1. The effect of luminosity on the mass–radius relation, where ρ_c , T_c , and M' are, respectively, the central density, central temperature, and mass, when $dT/dr = 0$ below envelope; R_* , ρ_* , and T_* are the interface radius, density, and temperature, respectively; and M is the mass for $dT/dr \neq 0$ throughout.

$R/1000$ km	L/L_{\odot}	$\rho_c/10^6$ g cm $^{-3}$	$T_c/10^6$ K	$R_*/1000$ km	$\rho_*/10^6$ g cm $^{-3}$	$T_*/10^8$ K	M'/M_{\odot}	M/M_{\odot}
20	10^{-4}	0.0983	8.34	16.55	0.0011	0.083	0.165	0.24
	10^{-2}	0.212	27.39	13.99	0.0068	0.274	0.265	0.37
9.645	10^{-4}	2.36	5.92	9.442	0.000 68	0.059	0.545	0.7
	10^{-2}	3.15	21.29	9.03	0.0047	0.213	0.615	0.86
4.968	10^{-4}	55.35	4.85	4.95	0.0005	0.0485	1.09	1.24
	10^{-2}	60.29	17.97	4.89	0.0036	0.18	1.11	1.37
2.068	10^{-4}	1962	4.54	2.0651	0.000 46	0.0454	1.381	1.5
	10^{-2}	2019	16.89	2.0572	0.0034	0.169	1.385	1.61

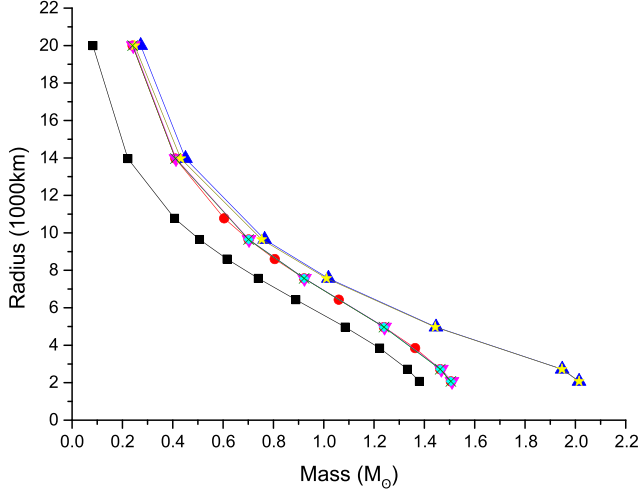


Figure 3. The effect of magnetic field and luminosity on the mass–radius relation, for Chandrasekhar’s results, without thermal and field contributions (black squares), and $dT/dr \neq 0$ throughout for $(B_s, B_0) = (0, 0)$ G (red circles), $(10^9, 10^{14})$ G (blue upward triangles), $(10^9, 10^{13})$ G (magenta downward triangles), $(10^9, 10^{12})$ G (sky diamonds), $(10^7, 10^{14})$ G (yellow stars), and $(10^7, 10^{12})$ G (green cross). Except for Chandrasekhar’s results, the luminosity is chosen to be $10^{-4} L_\odot$.

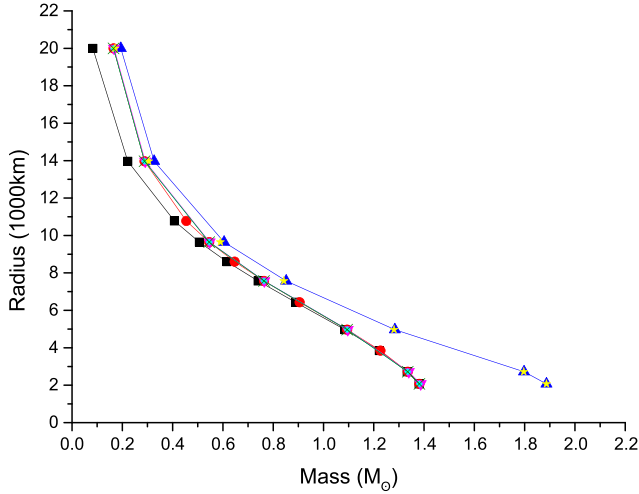


Figure 4. The effect of magnetic field and luminosity on the mass–radius relation, for Chandrasekhar’s results, without thermal and field contributions (black squares), and for $dT/dr = 0$ from the interface to the centre with $(B_s, B_0) = (0, 0)$ G (red circles), $(10^9, 10^{14})$ G (blue upward triangles), $(10^9, 10^{13})$ G (magenta downward triangles), $(10^9, 10^{12})$ G (sky diamonds), $(10^7, 10^{14})$ G (yellow stars), and $(10^7, 10^{12})$ G (green cross). Except for Chandrasekhar’s results, the luminosity is chosen to be $10^{-4} L_\odot$.

the high-mass (density) regime, all low magnetic field mass–radius curves practically overlap along with that of Chandrasekhar.

Notice that the central density of highly magnetized white dwarfs is higher than that of the non-magnetized ones in order to compensate for the additional magnetic pressure. This is because the contribution of the magnetic field to the total pressure is larger than that to total density. Interestingly, white dwarfs with a central field of about 10^{14} G are significantly super-Chandrasekhar with masses exceeding $2 M_\odot$ at high central densities.

Table 2 shows how the presence of a magnetic field increases the central density of white dwarfs and so increases their mass. Intu-

itively, we know that the presence of the magnetic field decreases the interface radius because it affects dT/dr directly, similarly to the effect of luminosity on the system. Therefore, higher magnetic fields have larger effects. Nevertheless, it is crucial to know that the effective strength of the magnetic field is defined by both its B_s and B_0 . If we decrease B_0 for a particular B_s , the results become closer to the non-magnetic case. But for a high B_0 , decreasing B_s also leads to a larger interface radius than the non-magnetic case, as seen in Table 2 when compared with the respective cases in Table 1.

4 SUPPRESSION OF LUMINOSITY DUE TO MAGNETIC FIELD

From the conservation of energy, in order to assure stability, the increase in the magnetic energy in the white dwarf has to be compensated for by a decrease in thermal energy for a given gravitational energy. This, in turn, decreases the measure of luminosity and, hence, the temperature. This is particularly the case in lower density, higher radius white dwarfs, when the thermal, magnetic, and gravitational energies are comparable, i.e. when the ideal gas and magnetic pressures are comparable and the degenerate gas pressure inside white dwarfs is not too high compared to them. From Figs 2–4, we have noticed that strong central magnetic fields corresponding to $B_0 = 10^{14}$ G show a deviation from the non-magnetized mass–radius relation. We explore these cases further and the results are listed in Table 3. We find that for larger radius, lower density white dwarfs, a slight decrease in luminosity leads to the mass and central density of the magnetized white dwarf comparable to its non-magnetic counterpart. This is still in the observable range.

However, the situation differs for higher density smaller radius white dwarfs, where the thermal pressure inside turns out to be significantly subdominant; hence, decreasing thermal energy does not affect its mass. Moreover, as the magnetic pressure contributes to magnetostatic balance with increasing mass for a radius same as the non-magnetic white dwarf, its central density increases compared to its non-magnetic counterpart in order to satisfy mass equation; see Table 3. Therefore, for smaller radius, higher density white dwarfs, even if the luminosity decreases considerably (10^{-12} – $10^{-20} L_\odot$), the mass of the magnetized white dwarf remains quite high compared to its non-magnetic counterpart. This leads to an extended branch in the mass–radius relation, which is absent in the non-magnetic counterpart. This is seen in Fig. 5. This implies that there can be white dwarfs with high magnetic field strengths (and high mass) but these are too faint to detect.

5 DISCUSSION

The SDSS data show that there are a large number of large-radius and small-mass white dwarfs whose masses are high compared to Chandrasekhar’s mass–radius relation. Nevertheless, Boshkayev et al. (2016) showed that the finite temperature electron-degenerate EoS at higher temperatures could explain these observations. We also obtain similar results for no and weak magnetic fields by appropriately introducing the photon-diffusion equation (2). Moreover, our solutions self-consistently define the interface between the interior degenerate core and outer envelope with ideal gas layers.

In addition, we obtain super-Chandrasekhar non-magnetic white dwarfs for a constant luminosity of, say, $10^{-2} L_\odot$, hypothesizing $dT/dr \neq 0$ throughout. This particularly shows the effects of very high temperatures, which arise because of the non-zero dT/dr throughout and high surface temperature, on small radius white dwarfs. Further, in the presence of weak magnetic fields, we obtain

Table 2. The effect of magnetic field for a particular luminosity ($10^{-4} L_{\odot}$) on the mass–radius relation, where ρ_c , T_c , and M' are, respectively, the central density, central temperature, and mass, when $dT/dr = 0$ below the interface; R_* , ρ_* , and T_* are the interface radius, density, and temperature, respectively; and M is the mass for $dT/dr \neq 0$ throughout.

$R/1000$ km	$(B_s, B_0)/G$	$\rho_c/10^6$ g cm $^{-3}$	$T_c/10^6$ K	$R_*/1000$ km	$\rho_*/10^6$ g cm $^{-3}$	$T_*/10^8$ K	M'/M_{\odot}	M/M_{\odot}
20	$(10^9, 10^{14})$	0.136	8.04	15.93	0.001 08	0.0804	0.194	0.27
	$(10^9, 10^{13})$	0.102	8.3	16.46	0.001 14	0.083	0.168	0.24
	$(10^7, 10^{14})$	0.1	8.27	16.64	0.001 1	0.0827	0.171	0.25
9.645	$(10^9, 10^{14})$	2.68	5.8	9.346	0.000 66	0.058	0.604	0.76
	$(10^9, 10^{13})$	2.38	5.92	9.429	0.000 683	0.059	0.547	0.70
	$(10^7, 10^{14})$	2.5	5.79	9.458	0.000 66	0.0579	0.59	0.75
4.968	$(10^9, 10^{14})$	59.17	4.7	4.9342	0.000 49	0.047	1.284	1.44
	$(10^9, 10^{13})$	55.483	4.85	4.944	0.000 51	0.0485	1.096	1.24
	$(10^7, 10^{14})$	58.26	4.64	4.949	0.000 475	0.0465	1.28	1.44
2.068	$(10^9, 10^{14})$	2502.5	4.23	2.0642	0.000 43	0.0423	1.887	2.01
	$(10^9, 10^{13})$	1966.5	4.54	2.06486	0.000 462	0.0454	1.39	1.51
	$(10^7, 10^{14})$	2490.3	4.16	2.066	0.000 414	0.0416	1.887	2.01

Table 3. Mass and central density of white dwarf from conservation of magnetic and thermal energies for different field profiles and radii.

$R/1000$ km	$(B_s, B_0)/G$	Without interface			With interface			$\rho_c/10^6$ g cm $^{-3}$	$\rho_c^{\text{original}}/10^6$ g cm $^{-3}$
		L/L_{\odot}	M/M_{\odot}	$M_{\text{original}}/M_{\odot}$	L/L_{\odot}	M/M_{\odot}	$M_{\text{original}}/M_{\odot}$		
20	$(10^9, 10^{14})$	2×10^{-5}	0.244	0.24	8×10^{-6}	0.166	0.165	0.106	0.0983
20	$(10^7, 10^{14})$	7×10^{-5}	0.242	0.24	7×10^{-5}	0.166	0.165	0.095	0.0983
13.965	$(10^9, 10^{14})$	2×10^{-5}	0.416	0.411	10^{-6}	0.287	0.288	0.3934	0.4095
13.965	$(10^7, 10^{14})$	5×10^{-5}	0.415	0.411	3×10^{-5}	0.289	0.288	0.3854	0.4095
9.645	$(10^9, 10^{14})$	5×10^{-6}	0.701	0.701	10^{-12}	0.566	0.545	2.29	2.36
9.645	$(10^7, 10^{14})$	10^{-5}	0.702	0.701	10^{-12}	0.551	0.545	2.121	2.36
7.57	$(10^9, 10^{14})$	5×10^{-7}	0.923	0.922	10^{-12}	0.829	0.763	7.873	7.738
7.57	$(10^7, 10^{14})$	10^{-6}	0.924	0.922	10^{-12}	0.818	0.763	7.7563	7.738
4.968	$(10^9, 10^{14})$	10^{-16}	1.278	1.239	10^{-16}	1.273	1.094	57.19	55.35
4.968	$(10^7, 10^{14})$	10^{-12}	1.285	1.239	10^{-12}	1.270	1.094	56.35	55.35
2.7215	$(10^9, 10^{14})$	10^{-12}	1.807	1.463	10^{-16}	1.794	1.335	720.89	686.96
2.7215	$(10^7, 10^{14})$	10^{-12}	1.807	1.463	10^{-12}	1.793	1.335	718.62	686.96
2.068	$(10^9, 10^{14})$	10^{-20}	1.886	1.505	10^{-16}	1.886	1.381	2473.8	1962
2.068	$(10^7, 10^{14})$	10^{-20}	1.886	1.505	10^{-16}	1.886	1.381	2462.4	1962

Notes. Here M_{original} and ρ_c^{original} denote the mass and central density of the white dwarf in the absence of magnetic field with $L = 10^{-4} L_{\odot}$. Also, the central densities here are only for the cases with interface.

the same mass–radius relations as for the non-magnetic cases when $dT/dr = 0$ below the interface. However, in cases of stronger magnetic fields, whether $dT/dr = 0$ below the interface or not, we obtain super-Chandrasekhar masses. Thus, our results, which depend on the photon-diffusion equation, suggest the existence of super-Chandrasekhar white dwarfs for three different cases: (1) constant higher luminosity (about $10^{-2} L_{\odot}$) with non-zero dT/dr throughout, (2) strong magnetic field with non-zero dT/dr throughout, and (3) strong magnetic field with $dT/dr = 0$ below the interface radius. While the two former situations may be implausible because then non-magnetic and non-rotating white dwarfs might have super-Chandrasekhar mass, the last is quite plausible. These could very well be the candidates for super-Chandrasekhar progenitors of overluminous SNe Ia.

Another interesting result is that, for the white dwarfs with smaller radii and stronger magnetic fields, the decrease in luminosity does not lead to the merging of the mass–radius relation of white dwarfs with that of their non-magnetic counterparts, leaving super-Chandrasekhar white dwarfs separate in the mass–radius relation. Hence, there can be super-Chandrasekhar magnetic white dwarfs which are so dim or have very low luminosity (as little as

$10^{-20} L_{\odot}$), which we have missed from detection. But for larger radii, depending on their magnetic field strengths, we see the mass–radius relation merging with the non-magnetic counterpart. Hence, with improved observational techniques and instruments, these still hold a chance to be observed because their luminosity is of the order of 10^{-5} – $10^{-8} L_{\odot}$.

There are a few important points to be stressed. In our case, the EoS for the electron-degenerate pressure is temperature independent and it becomes very important to check for its validity when we are solving for dT/dr . In order to validate the choice, the Fermi energy E_F has to be much greater than the thermal energy of the matter. For all the cases considered here, this condition has always been satisfied, at least in the inner degenerate core. It is observed that $E_F/kT \approx 5$ at the interface, and it increases below the interface.

We have attempted to explore the idea of including the energy conservation equation $dL(r)/dr = 4\pi r^2 \rho(r) \epsilon(r)$, where $\epsilon(r)$ is the power produced per unit mass of stellar material in the system, in place of constant luminosity. However, because white dwarfs do not have a consistent energy production mechanism, our model equation does not perform adequately compared to our assumption of constant luminosity. Further, at high temperature, energy losses

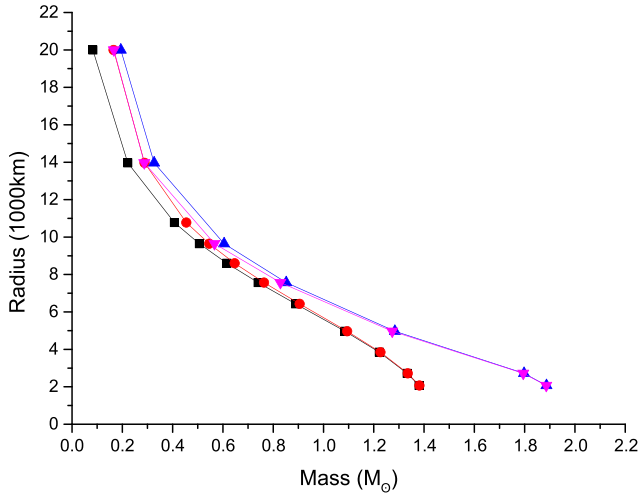


Figure 5. The effect of magnetic field optimizing luminosity to attempt to match with Chandrasekhar’s mass–radius relation (black squares), for $(B_s, B_0) = (10^9, 10^{14})$ G (magenta downward triangles), while the lines with red circles and blue upward triangles represent the results with $L = 10^{-4} L_\odot$ for $(B_s, B_0) = (0, 0)$ and $(10^9, 10^{14})$ G respectively. All cases correspond to $dT/dr = 0$ below the interface radius. See Table 3 for specific luminosities.

due to neutrino emission may turn out to be important (depending on the temperature and its variation), which we also have omitted from this work. Moreover, we have not included possible convection in our computation, assuming that the strong field inhibits its effect. However, convection may transfer significant energy (Valyavin et al. 2014) in non-magnetic and weakly magnetized white dwarfs that we keep considering for comparison, particularly for $dT/dr \neq 0$ throughout. In future, all of these physics will be appropriately considered in a more sophisticated model framework.

In addition to this, we have used a Newtonian framework throughout our work. This is practically a valid assumption for the present purpose of white dwarfs. We eventually should explore the Tolman–Oppenheimer–Volkoff equation (Oppenheimer & Volkoff 1939) along with temperature gradient and necessary related physics. Nonetheless, in the case of white dwarfs, $2GM/c^2R$ is quite small, and this favours the choice of a Newtonian framework.

The work may be further extended for higher magnetic fields, where Landau quantization becomes important. Nonetheless, this work, in itself, is quite unique because we could define an interface between the degenerate core and outer ideal gas envelope self-consistently and obtain mass–radius and luminosity relationships including the radiative transport equation in the magnetized and non-magnetized cases, which are in accordance with observations. Moreover, we have obtained a unique result that, in the presence of strong magnetic fields, small-radius white dwarfs can always be undetected because they may be too dim to detect, even if they are on the similar mass–radius track as their non-magnetic counterparts.

6 CONCLUSION

Observations of the light curves of overluminous peculiar SNe Ia imply the presence of super-Chandrasekhar white dwarfs but there has been no direct observation of such a white dwarf. Moreover, many theories have been put forward to explain the Chandrasekhar mass-limit violation. These include the white dwarfs being highly magnetized and rotating. We argue that highly magnetized white

dwarfs’ luminosities can be suppressed to the extent that they are practically hidden, and cannot be detected. In the future, through gravitational wave detectors such as LISA, eLISA, and a few others, their presence may be detected (Kalita & Mukhopadhyay 2019).

Most of the studies of white dwarfs, so far, assumed beforehand the existence of an interface between the two pressure components, electron-degenerate pressure, and ideal gas pressure. We have shown that the interface can be self-consistently found, for magnetic or non-magnetic white dwarfs.

ACKNOWLEDGEMENTS

AG and BM would like to thank Mukul Bhattacharya of the University of Texas, Austin, for discussion at the initial phase of this work. This work was partly supported by a project of Department of Science and Technology with Grant No. DSTO/PPH/BMP/1946 (EMR/2017/001226). CAT thanks Churchill College for his fellowship.

REFERENCES

- Bandyopadhyay D., Chakrabarty S., Pal S., 1997, *Phys. Rev. Lett.*, 79, 2176
 Bhattacharya M., Mukhopadhyay B., Mukerjee S., 2018, *MNRAS*, 477, 2705
 Boshkayev K., Rueda J. A., Ruffini R., Siutsou I., 2013, *ApJ*, 762, 117
 Boshkayev K. A., Rueda J. A., Zhami B. A., Kalymova Z. A., Balgymbekov G. S., 2016, *Int. J. Mod. Phys.: Conf. Ser.*, 41, 1660129
 Canuto V. M., Mazzitelli I., 1992, *ApJ*, 389, 724
 Carvalho G. A., Arbañil J. D. V., Marinho R. M., Malheiro M., 2018, *Eur. Phys. J. C*, 78, 411
 Chandrasekhar S., 1935, *MNRAS*, 95, 207
 Das U., Mukhopadhyay B., 2012, *Phys. Rev. D*, 86, 042001
 Das U., Mukhopadhyay B., 2013, *Phys. Rev. Lett.*, 110, 071102
 Das U., Mukhopadhyay B., 2014, *J. Cosmol. Astropart. Phys.*, 2014, 050
 Das U., Mukhopadhyay B., 2015, *J. Cosmol. Astropart. Phys.*, 2015, 016
 Das U., Mukhopadhyay B., Rao A. R., 2013, *ApJ*, 767, L14
 Franzon B., Schramm S., 2015, *Phys. Rev. D*, 92, 083006
 Howell A. D. et al., 2006, *Nature*, 443, 308
 Kalita S., Mukhopadhyay B., 2019, *MNRAS*, 490, 2692
 Koester D., Chanmugam G., 1990, *Rep. Prog. Phys.*, 53, 837
 Mukhopadhyay B., Rao A. R., 2016, *J. Cosmol. Astropart. Phys.*, 2016, 007
 Mukhopadhyay B., Rao A. R., Bhatia T. S., 2017, *MNRAS*, 472, 3564
 Oppenheimer J. R., Volkoff G. M., 1939, *Phys. Rev.*, 55, 374
 Otoniel E., Franzon B., Carvalho G. A., Malheiro M., Schramm S., Weber F., 2019, *ApJ*, 879, 46
 Scalzo R. A. et al., 2010, *ApJ*, 713, 1073
 Shapiro S. L., Teukolsky S. A., 1983, *Black Holes, White Dwarfs and Neutron Stars: The Physics of Compact Objects*. Wiley, New York
 Silverman J. M., Ganeshalingam M., Li W., Filippenko A. V., Miller A. A., Poznanski D., 2011, *MNRAS*, 410, 585
 Sinha M., Mukhopadhyay B., Sedrakian A., 2013, *Nucl. Phys. A*, 898, 43
 Solanki S. K., 2003, *A&AR*, 11, 153
 Subramanian S., Mukhopadhyay B., 2015, *MNRAS*, 454, 752
 Valyavin G. et al., 2014, *Nature*, 515, 88
 Vanlandingham K. M. et al., 2005, *AJ*, 130, 734
 Ventura J., Potekhin A., 2001, *The Neutron Star–Black Hole Connection*. Kluwer, Dordrecht

APPENDIX A: REPRESENTATIVE SAMPLE CASE STUDY

Here we outline the process of obtaining the interface radius for a particular case. The following example is for a white dwarf or B-WD with $R = 4968$ km in the presence of magnetic field $(B_s, B_0) = (10^9, 10^{14})$ G with luminosity $10^{-4} L_\odot$.

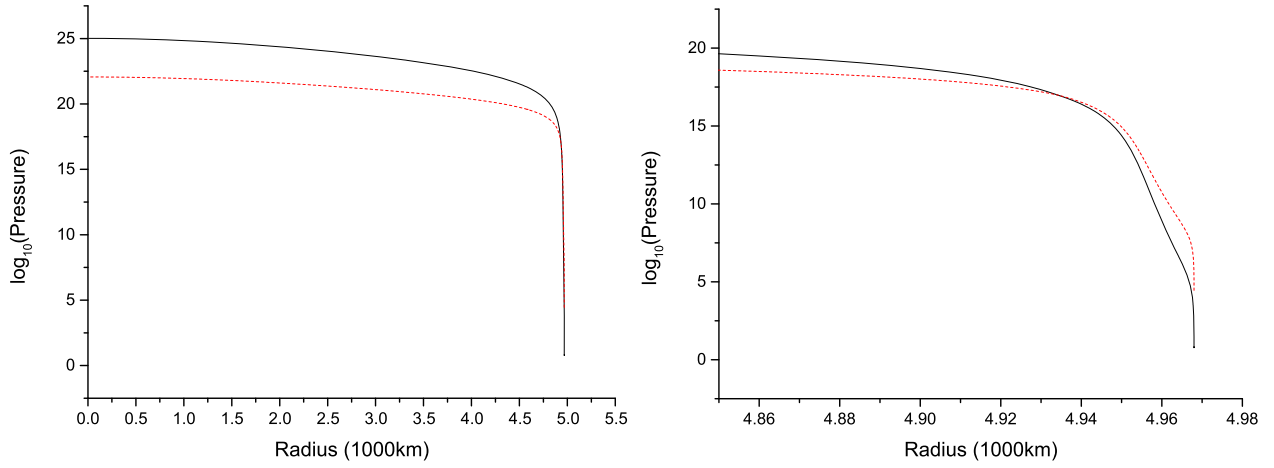


Figure A1. The variation of electron-degenerate pressure (solid black line) and ideal gas pressure (dashed red line) as functions of radius, when $dT/dr = 0$ below the interface. The right-hand panel is the same as the left-hand panel, but zoomed in the outer region close to the surface. Note that the ideal gas pressure takes over the electron-degenerate pressure around 4934 km.

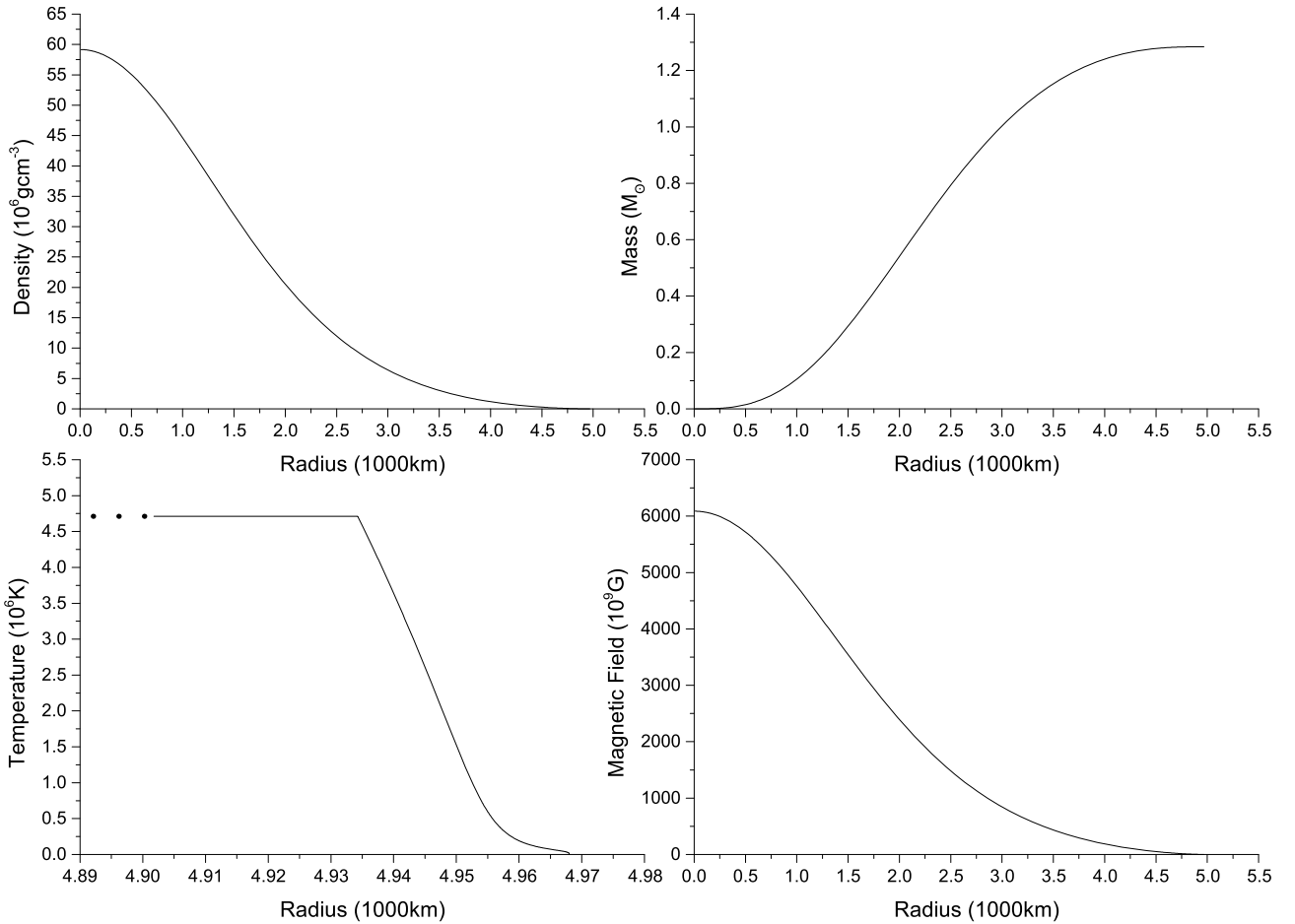


Figure A2. For a particular mass–radius relation, the variations of density (top left-hand panel), mass (top right-hand panel), temperature (bottom left-hand panel), and magnetic field (bottom right-hand panel), as functions of radius in a white dwarf. Note that the temperature varies only on the surface layer above 4934 km (interface) and remains constant from the interface to centre, part of which has been depicted.

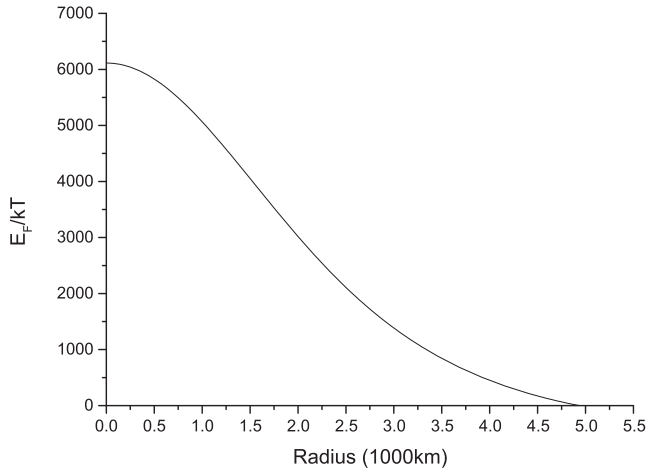


Figure A3. The variation of ratio of the Fermi energy to thermal energy as a function of radius.

In Fig. A1, we show the various pressure profiles and it is seen that roughly at 4934 km, the ideal gas pressure overpowers the electron degeneracy pressure. Hence, this radius can be defined as the interface radius for this case. Fig. A1 clearly confirms the dominance of the electron-degenerate matter in the core about three orders of magnitude over the ideal gas pressure. Further applying $dT/dr = 0$ below this interface radius, we obtain the mass for a white dwarf with $R = 4968$ km; see Table 2. Fig. A2 represents the profiles for density, mass, temperature, and magnetic field as functions of radius. Density and magnetic field have roughly the same profiles because the strength of magnetic field is density dependent. Fig. A3 also confirms that Fermi energy is significantly dominant over thermal energy, assuring the validity of zero-temperature EoS.

This paper has been typeset from a $\text{\TeX}/\text{\LaTeX}$ file prepared by the author.